International Journal of Thermofluids 10 (2021) 100074

Contents lists available at ScienceDirect

International Journal of Thermofluids

journal homepage: www.elsevier.com/locate/ijtf

Evaluating velocity and temperature fields for Ranque–Hilsch vortex tube using numerical simulation

Ahmad M. Alsaghir, Mohammad O. Hamdan, Mehmet F. Orhan*

Department of Mechanical Engineering, American University of Sharjah, P.O. Box: 26666, Sharjah, United Arab Emirates

ARTICLE INFO

Article History:
Received 1 February 2021
Revised 17 February 2021
Accepted 23 February 2021
Available online 2 March 2021

Keywords:
Vortex tube flow field
Flow structure inside vortex tube
Energy separation
Turbulence modeling of vortex tube

ABSTRACT

In this study, a three-dimensional numerical investigation is carried out to study the flow field inside a Ranque-Hilsch vortex tube (RHVT) model. Flow parameters such as velocity, temperature, and pressure are plotted at various locations inside the tube. The study reports the effect of cold mass fraction on the energy separation of vortex tube . The results show that the flow inside RHVT consists of a free vortex from r/R=0 to 0.9 and a force vortex from r/R=0.9 to 1 and that heat transfer occurs from the inner core to the periphery of the tube. Furthermore, it is observed that the minimum cold temperature and the maximum hot temperature are achieved at different mass fractions, 0.19 and 0.8, respectively.

1. Introduction

Thermal management is achieved using different tools such as heat exchanger [1], vortex tube [2], fins [3], heat pipes [4] and phase change material [5]. A vortex tube (VT) is a thermo-fluidic device that is capable of splitting a pressurized fluid into hot and cold currents simultaneously, without any moving parts or chemical reactions. It was accidently discovered by a French scientist in 1933 [6]. In 1947, a German scientist modified the structural parameters of the tube to improve its performance [7]. VT consists of inlet nozzles where fluid is admitted in a tangential manner (known as vortex generator), a strait tube, a cold orifice, and a hot orifice with a control valve to adjust the mass flow fractions. VT has a wide range of spot cooling applications. For instance, it is used for cooling milling machining to preserve the properties of the work piece and protect the cutting tools [8,9], cooling the working suits of mines workers [10], solid–liquid separators [11], convex mirror cooling [12] or other air-conditioning systems [13]. Shmroukh et al. [14] have reported the feasibility of using a vortex tube in water desalination.

Currently, there is no consensus on how the energy separation effect in VT takes place. Nonetheless, many theories have been proposed to explain this phenomenon [15–17]. For instance, the viscous shear theory suggests that the angular velocity increases towards the center and tends to conserve the angular momentum of the fluid, which in turn transfers the excess kinetic energy to the periphery of the tube through the shear force [15,16]. Another theory has proposed [17] that the cause of temperature difference is a phenomenon named “acoustic streaming”. This phenomenon relates the acoustics waves generated at the hot outlet to the formation of some secondary flows and turbulent eddies inside the tube.

Hilsh’s modifications [7] and the advantages of VT have motivated the scientific community to look for further ways to improve its operating efficiency. Many experimental and numerical studies have been carried out to investigate the effect of the structural parameters as well as the operating conditions on the performance of the vortex tube. Hamdan et al. [2] have experimentally investigated the effect of 4 different design parameters, namely (1) inlet pressure, (2) tube length, (3) tube diameter, and (4) tube tapered angle, on the performance of the vortex tube. It was reported that the inlet pressures rise achieves a greater temperature difference until a peak value, after which the performance starts to deteriorate [2]. It was suggested that the performance deterioration occurs due to the inlet nozzles choked condition. The effect of tube’s roughness has been investigated by Parulekar [18] and it was reported that the efficiency of VT decreases as the tube’s roughness increases. Eiamsa-ard et al. [19] have investigated the effect of number of inlet nozzles on the temperature separation. The measurements showed that the energy separation increases with more nozzles and this improvement has been referred to the increase in the swirl intensity. Similar results have been reported by Dincer et al. [20] who have stated that the efficiency of the vortex tube with 4 and 6 inlet nozzles are better than with 2 inlet nozzles.

Beside the number of nozzles, their size also has a great effect on the separation. Mohammadi et al. [21] have revealed that a smaller nozzle area results in a higher separation magnitude. Also, Celik et al.

* Corresponding author.
E-mail addresses: b00079096@aus.edu (A.M. Alsaghir), mhamdan@aus.edu (M.O. Hamdan), morhan@aus.edu (M.F. Orhan).

https://doi.org/10.1016/j.ijft.2021.100074

Nomenclature

$C_{1\varepsilon}$	Constant
$C_{2\varepsilon}$	Constant
$C_{3\varepsilon}$	Constant
C_p	Specific heat
G_b	Generation of turbulence kinetic energy due to buoyancy
G_k	Generation of turbulence kinetic energy
P_{in}	Inlet pressure
P_{ref}	Reference pressure
S_k	Turbulence kinetic energy user source term
S_ε	User source term
T_{in}	Inlet temperature
V_{in}	Inlet velocity
V_t	Tangential velocity
V_z	Axial velocity
Y_M	Contribution of the fluctuating dilatation to the overall dissipation rate
L	Length of the tube
R	Radius of the tube
k	Turbulence kinetic energy
l	Distance from the origin
r	Distance from the center line

Greek Symbols

ρ	Density
μ	Dynamic viscosity
ε	Turbulence dissipation rate
Δ	Change in value
σ_ε	Turbulent Prandtl number for ε
σ_k	Turbulent Prandtl number for k

Abbreviations

RHVT	Ranque-Hilsch vortex tube
VT	Vortex tube
COP	Coefficient of performance
Ma	Mach number

[22] have investigated the effect of nozzle to tube's diameter ratio. The results showed the highest cold temperature difference at an optimum diameter ratio of 0.64. Another study [23] has presented that increasing the number of inlet jets leads to hotter and colder currents at the outlets, which does not necessary leads to a rise in the heating and cooling load of the VT. It has also been reported that the minimum and the maximum temperatures do not occur at the same mass fractions.

Working fluid is another crucial parameter in the separation. Kirmaci [24] has tested oxygen as a working fluid and the measurements showed that it gives higher temperature difference than air. After testing various type of refrigerants, Han et al. [25] have achieved the highest temperature difference by using R728. Kaya et al. [26] have tested the performance of serial and parallel connected RHVT, using carbon dioxide (CO_2) as a working fluid . They have reported that the efficiency of the parallel connection is higher than that of serial connection, and using CO_2 gives relatively lower temperature difference than oxygen and air.

Employing their ability to provide details of flow structure under different operating conditions, many scientists have used numerical simulation to better understand the flow structure inside the VT. For instance, Aljuwayhel et al. [27] have used 2D axisymmetric model to numerically investigate the energy separation in a VT. It was reported that the magnitude of radial velocity component was very small compared to the axial and swirl velocities. Also, the static temperature decreased in the radial direction, which leaded to heat transfer in the radial direction. Skye et al. [28] has used ANSYS fluent package to study VT flow and has tested two numerical turbulence models, namely, standard k-ε and RNG k-ε. By comparing the numerical models with the experimental measurements, it has been observed that both models under predict the outlet's temperatures, the standard k-ε results being closer to the experimental values. Baghdad et. al [29] have investigated the impact of the adiabatic walls assumption on the outlets temperature difference. It was found that at small cold mass fraction, this assumption has a mild influence compare to that at high mass fraction.

Shamsoddini et al. [30] have used a 3D numerical model to investigate the effect of number of inlet jets on the streamlines. It has been concluded that the streamlines followed a similar pattern as in axisymmetric assumption only in case of large number of nozzles. Different turbulence models, namely standards k-ε, standard k-ω, SST k-ω, and RSM, have been tested by Baghdad et al. [31]. Then, the outcomes have been compared with published experimental data [32]. The researchers have found that all of the turbulence models are able to predict the energy separation phenomenon. However, only the RSM model was in agreement with the experimental temperature difference. These findings match the outcomes of [33] who compares the results of RNG $k-\varepsilon$,and RSM RANS models with that of LES model.

Behera et al. [34], using computational fluid dynamics (CFD) simulation, have reported that a secondary flow structure may cause deterioration in the VT performance. Another numerical investigation [35], using standards k-ε, RNG k-ε, standard k-ω, and SST k-ω, has showed that all models are in good agreement with the experimental work, except the RNG k-ε model. This result contradicts with [26] that has numerically investigated the energy separation in vortex tube using k-ε and RNG k-ε, and reported that the RNG k- ε provided a better energy separation prediction. Thakare et al. [36] have investigated the energy separation of VT using different turbulence models. Their results have pointed out that the Spalart–Allmaras model over predicted the cold and hot temperature, while the RSM under predicted these temperatures.

Bramo et al. [37] have used numerical simulations to test the effect of the diameter and length of the tube on the performance of the VT. They have claimed that the best performance was obtained at a length to diameter ratio of 9.3. Furthermore, the study has reported that the temperature difference between the cold and the hot outlets increases with the length of the tube. Eiamsa-ard et al. [38] have numerically studied the effect of both the numerical scheme (hybrid, upwind, and second order upwind) and the turbulence models (k-ε and algebraic stress model (ASM) models) on the calculation of energy separation in a parallel flow vortex tube. They have reported that the three numerical schemes have no effect on the prediction of the temperature difference. Farouk et al. [39] have utilized the LES model to examine the energy separation in axisymmetric VT model. The results have stated that the minimum total temperature occurred near the tube center, while the maximum temperature near the tube periphery. Furthermore, it was indicated that the minimum value of static and total temperatures were close to each other. Farouk et al. [39] have reported that the difference between static and total temperatures at the periphery of the tube was due to the conversion of kinetic energy into thermal energy. In this regard, another numerical study [40] has used standard k-ε turbulence model and showed a good agreement with experimental results.

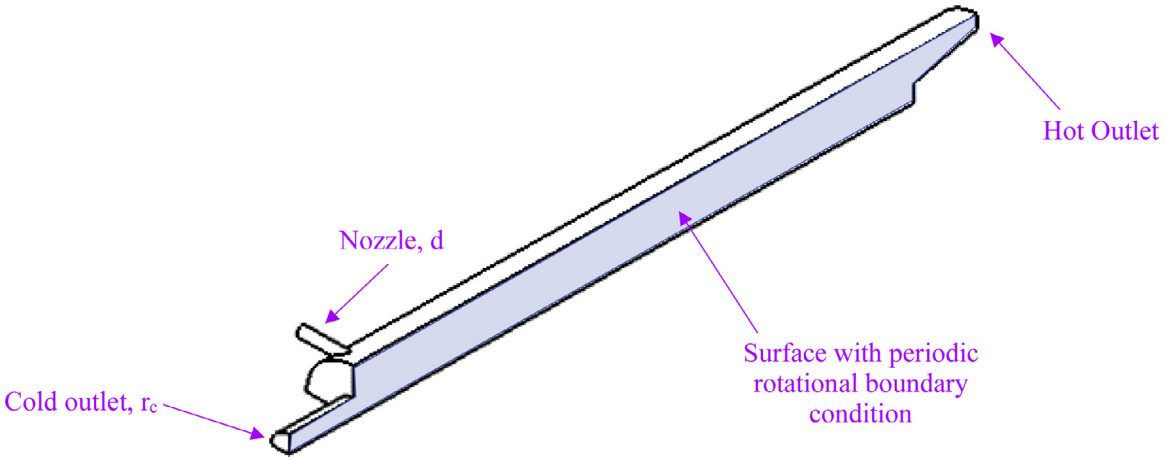

Fig. 1. A three-dimensional model of the vortex tube in 90° sector.

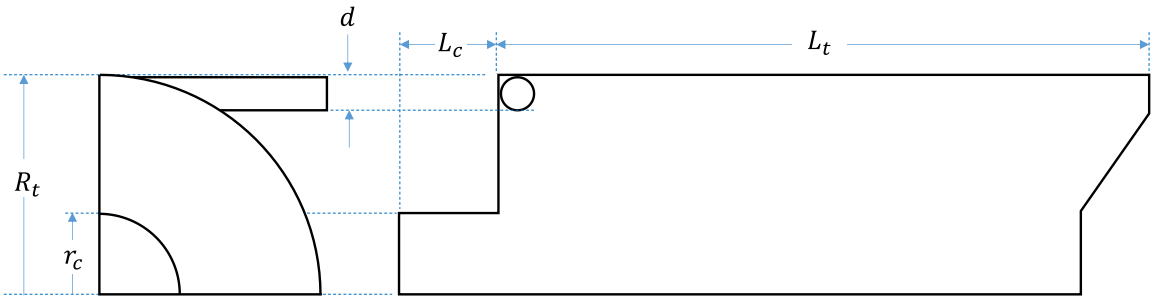

Fig. 2. A two-dimensional schematic of the vortex tube with its main dimensions.

To help aforementioned ongoing efforts, the objective of this study is to numerically investigate the flow structure inside a vortex tube. In this regard, a three-dimensional k-ε turbulent model is used to study the flow and energy separation due to the vortex flow. The study also aims to examine the impact of wall treatments on the numerical results, mainly standard and enhanced wall treatments in properly predicting flow fields. The flow structure parameters such as the radial distribution of velocity, pressure, and temperature at different locations are evaluated. Furthermore, the effect of cold mass fraction is studied by changing the pressure of hot outlet. Finally, the inlet Mach number is reported at different inlet pressure.

2. Problem formulation

2.1. Computational domain

A schematic of the three-dimensional VT is shown in Fig. 1. The dimensions of the vortex tube used in this study are obtained from an earlier experimental study [41]. To reduce the computational time, a quarter of the model is simulated with a periodic rotational boundary condition. The dimensions used in the analysis are listed in Table 1 and are illustrated in Fig. 2. To simplify the generation of structured mesh, the 3D model is divided into three subdomains as shown in Fig. 3. The numerical model is generated using a commercial finite volume CFD software, ANSYS-fluent.

Table 1
Dimensions of the vortex tube.

Parameter	Dimension (mm)
Tube radius (R_t)	7.24
Tube length (L_t)	97
Cold outlet length (L_c)	10
Cold outlet radius (r_c)	2.715
Nozzle diameter (d)	1.6
Inlet pipe (D)	16

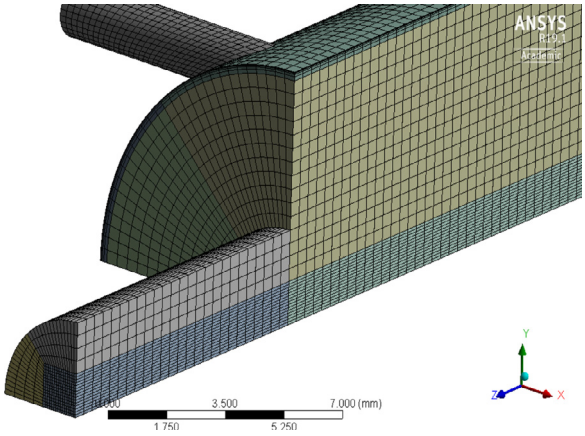

Fig. 3. Hexahedral mesh of modeled vortex tube.

2.2. Governing equations

In order to obtain flow structure and temperature of air flow in a vortex tube, one need to simultaneously solve the conservation equations with the ideal gas equation. Conservation of mass is formulated as,

$$\frac{\partial(\rho\overline{u}_i)}{\partial x_i} = 0 \tag{1}$$

while, conservation of momentum is,

$$\frac{\partial(\rho\overline{u}_i\overline{u}_j)}{\partial x_j} = -\frac{\partial\overline{p}}{\partial x_i} + \frac{\partial}{\partial x_j}\left[\mu\left(\frac{\partial\overline{u}_i}{\partial x_j} + \frac{\partial\overline{u}_j}{\partial x_i}\right) - \rho u_i' u_j'\right] \quad (2)$$

In this form of Navier-stocks equation the gravity force is neglected and only pressure is considered as body force. Also, conservation of energy is stated as,

$$\frac{\partial(\rho\overline{u}_j\overline{T})}{\partial x_j} = \frac{\partial}{\partial x_j}\left[\frac{\mu}{Pr}\left(\frac{\partial\overline{T}}{\partial x_j}\right) - \rho T' u_j'\right] \quad (3)$$

And, ideal gas equation of state is,

$$\overline{p} = \rho R\overline{T} \quad (4)$$

where $\overline{u}$, $\overline{T}$ and $\overline{p}$ are the time-averaged velocity, temperature, and pressure, respectively. The u_j' and T' represent the fluctuations in the velocity and temperature. The fluctuations terms in the momentum (Eq. 2) and energy (Eq. 3) equations are modelled using the Boussinesq hypothesis and the simple eddy diffusivity model, respectively, as shown in the following equations.

$$\rho u'_i u'_j = \mu_t\left(\frac{\partial u_i}{\partial x_j} + \frac{\partial u_j}{\partial x_i}\right) - \frac{2}{3}\rho k\delta_{ij} \quad (5)$$

$$\rho T'_i u'_j = -\frac{\mu_t}{\mathrm{Pr}_t}\left(\frac{\partial T}{\partial x_j}\right) \quad (6)$$

where, μ_t, k and Pr_t are the turbulent viscosity, turbulent kinetic energy and turbulent Prandtl number, respectively. The closure relationships of the turbulent Reynolds stresses $u_i' u_j'$ is assumed using $k-\varepsilon$ turbulence model.

2.3. k - ε turbulence model

This model is a two equations model where it solves two turbulence quantities, namely turbulence kinetic energy (k) and its dissipation rate (ε). The two transport equations used in this model with eddy viscosity are,

$$\frac{\partial(\rho k)}{\partial t} + \frac{\partial(\rho k u_i)}{\partial x_i} = \frac{\partial}{\partial x_i}\left[\left(\mu + \frac{\mu_t}{\sigma_t}\right)\frac{\partial k}{\partial x_i}\right] + -\rho\varepsilon \quad (7)$$

$$\frac{\partial(\rho\varepsilon)}{\partial t} + \frac{\partial(\rho\varepsilon u_i)}{\partial x_i} = \frac{\partial}{\partial x_i}\left[\left(\mu + \frac{\mu_t}{\sigma_\varepsilon}\right)\frac{\partial\varepsilon}{\partial x_i}\right] + C_{1\varepsilon}\frac{\varepsilon}{k}(G_k C_{3\varepsilon} G_b) - C_{2\varepsilon}\rho\frac{\varepsilon^2}{k} \quad (8)$$

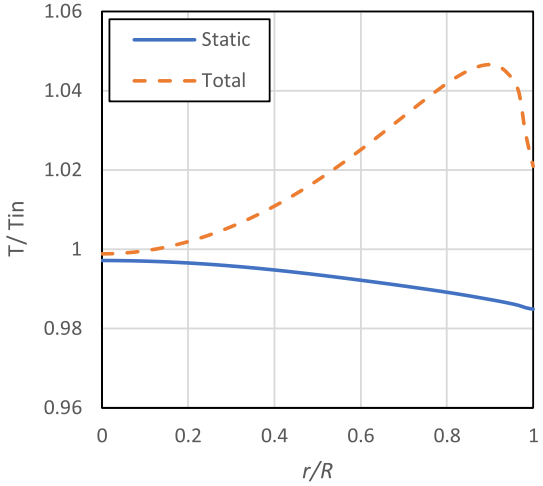

(a)

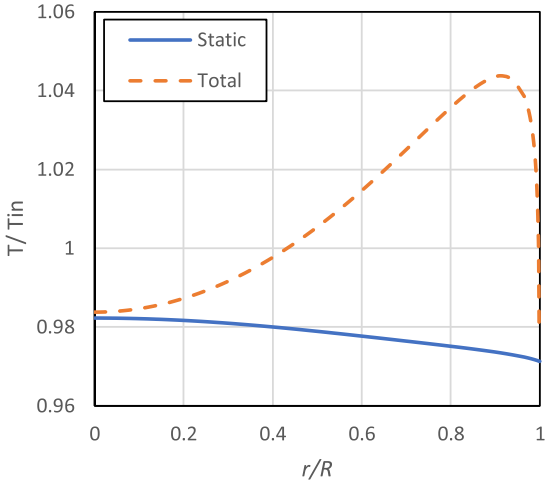

(b)

Fig. 5. Temperature profiles at l/L=0.62 using (a) standard wall function (b) enhanced wall function.

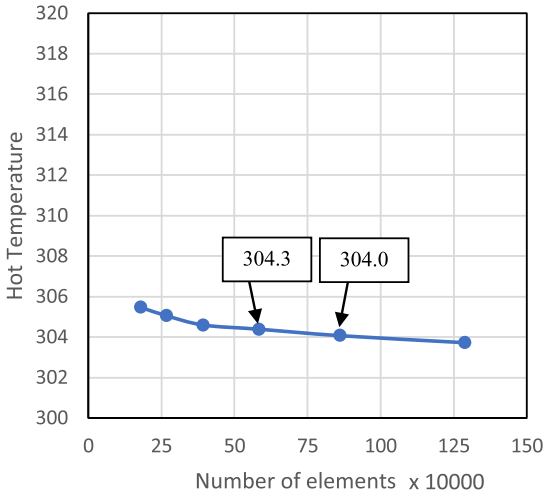

Fig. 4. Effect of mesh density on hot outlet temperature.

and

$$\mu_t = C_\mu\frac{\rho k^2}{\epsilon} \quad (9)$$

The default values are used for the empirical constants as follow: $C_\mu = 0.09$, $C_{1\varepsilon} = 1.44$, $C_{2\varepsilon} = 1.92$, $\sigma_t = 1.0$ and $\sigma_\varepsilon = 1.3$.

2.4. Mesh independence

Fig. 3 shows the hexahedral mesh that is used in this study. The first element size that ensure $Y^+ < 1$ is 0.01 mm. To assure that the obtained results are independent of the mesh density, a mesh independent study is also conducted based on the observation of hot outlet static temperature as shown in Fig. 4. It is clear that after 618,399 elements there is no substantial change in the static temperature. Therefore, a mesh with 618,399 elements (and 0.2 mm element size) is used to reduce the computational time.

2.5. Numerical setup and boundary conditions

A pressure solver is adopted to address the governing equation of this study. Air, with the default physical properties given by ANSYS, is used as a working fluid because Vortex tube is mostly used for spot

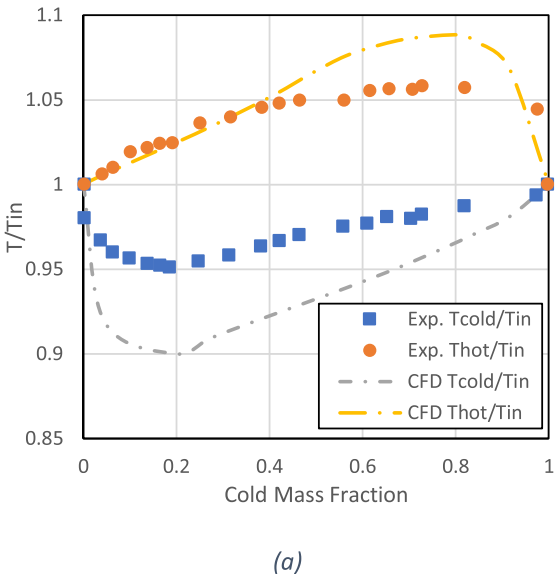

Fig. 6. Effect of cold mass fraction on the cold and hot outlet temperatures.

cooling, which makes air the best choice for thermal engineer due its availability and safety. Air density is calculated using the ideal gas law (Eq. 4). The convergence criteria are set to 10^{-9} for energy, while 10^{-6} for continuity, velocity, k, and ε. Since near wall region of the VT experiences very high velocities gradients, due to the high tangential velocities, standard and enhanced wall treatments are examined.

In the analysis, the boundary conditions enforced are,

- Smooth, no slip and adiabatic boundary conditions at the wall surfaces.
- Pressure inlet boundary condition of 4 bar at the inlet.
- Pressure outlet boundary condition of 0.5 bar at the hot outlet. This value is varied to test different mass fraction.
- Pressure outlet boundary condition of 0 bar at the cold outlet.
- Rotational periodic boundary condition about the axis of the tube.

3. Results and discussion

Fig. 5 illustrates the dimensionless temperature profiles in the radial direction for both standard and enhanced wall treatments. The dimensionless temperature is obtained dividing by the nozzle total inlet temperature. From the Fig., there is no doubt that the enhanced wall treatment offers more realistic results than the standard treatment. Fig. 5 (a) of the standard treatment suggests that the total and static temperature are not equal at the wall surfaces, regardless of no slip condition. This issue appears clearly with [42] who's results showed that the three velocity component, namely axial, radial, and tangential, are not equal to zero at the walls. In contrary and more accurately, the enhanced wall function in Fig. 5 (b) shows that the total and static temperature are equal as expected. The disagreement between the two wall treatments is due to the first element size. The smaller element size approaches closer to the wall surface with a zero velocity to obtain similar total and static temperature values. Therefore, the more accurate enhanced wall treatment is employed for the rest of the study.

Cold mass fraction is another common parameter used to describe a vortex tube performance. It is a fraction of the cold mass flow rate and the total mass entering the vortex tube ($\varepsilon = \dot{m}_c/\dot{m}_{in}$). The effects of cold mass fraction on the dimensionless outlet temperatures are shown in Fig. 6. The CFD results of this Fig. are in agreement with the experimental results of [41]. The numerical results in Fig. 6 (a) convince that the numerical model is capable of predicting the energy separation in the VT at different cold mass fractions. The inlet mass flow rate enters the VT in a tangential form at the room temperature and separates to cold and hot mass flow rates due to the vortex flow. The cold mass fraction varies at different hot outlet pressures. As hot outlet pressure increases, the nearby fluid reverses its direction toward the cold outlet and causes an increase in the cold mass fraction. The outlet temperatures and cold mass fraction have a non-monotonic relation. At zero cold mass fraction (ε = 0), the hot mass flow rate is equal to the inlet mass flow rate. On the other hand, at a cold mass fraction value of one (ε = 1), the entire inlet flow leaves through the cold outlet section. Therefore, no energy separation occurs at both extreme cold mass fraction values of zero or one, due to the single outlet. As shown in Fig. 6 (a), the hot and cold outlet temperatures reach to a peak value at different cold mass fractions.

As can be seen from Fig. 6, the coldest temperature ratio is obtained at a cold mass fraction value of 0.19, while the hottest is at 0.8. The experimental investigation in [41] suggests that the minimum temperature ratio and the maximum COP are obtained at different cold mass fractions, which was correlated in Eq. 9.

Fig. 7 (a) shows the tangential fluid velocity that varies with radius direction at different axial locations along the VT. This trend reveals the fact that the flow structure inside the vortex tube consists of a forced vortex (Rankin vortex) and free vortex. In the forced vortex region (r/R from 0 to 0.9), the fluid velocity increases linearly with radius, while in the free vortex region (r/R from 0.9 to 1.0), the fluid velocity decreases nonlinearly with radius and reaches to zero at the wall surfaces. Moreover, as seen from the Fig., the fluid velocity at the center decreases as the fluid moves towards the hot end and approaches to zero just before the hot valve, at z/L=0.88. Figs. 7 (b) and 7 (c) shows the axial and tangential velocities, respectively. In Fig. 7 (b), the inner region of the VT moves toward the cold outlet, while the fluid near the wall moves toward the hot outlet. The diameter of this inner region decrease as fluid moves towards the hot end. For example, at z/L=0.15 the radius ratio is 0.65, while at z/L=0.46 the radius ratio is about 0.5. At z/L=0.15, majority of fluid with a negative axial velocity either leave through the cold outlet or split into two portions. This motion is clearly visible in Fig. 8, where the fluid domain divides into three parts. The first portion circulates in the vortex generator region, the second part leaves through the cold end, and the third one leaves through the hot end. In the peripheral region the axial velocity magnitude decreases along the tube length, while increases in the central region. This trend is due to the momentum transfer from the outer (no slip condition at the wall surface) to the core region.

Fig. 7 (c) shows that the total fluid velocity varies in radial direction at different axial locations along the VT. Also, the fluid in the inner and outer regions rotates in the same direction. The tangential velocity component in Fig. 7 (a) is significantly larger than the axial component in Fig. 7 (b) and dominates the total velocity to have a similar profile. However, the total flow is dominated by the axial velocity near the center since the tangential velocity approaches to zero. In short, the inner region of the VT is dominated by the axial flow while the periphery region is dominated by tangential.

Fig. 9 (a) shows that the static pressure has a positive gradient in the radial direction and peaks at the wall surface. On the other hand, this gradient decreases as the fluid flows towards the hot end due to the decaying vortex, as shown in Fig. 7 (c). For example, at z/L=0.15 the difference between the central and the peripheral static pressures is the maximum. Then, this difference decreases along the tube and reaches to its minimum value at z/L=0.88. This trend indicates that, the angular velocity, hence the static pressure gradient can reach to zero for longer tubes. The radial density profile of the working fluid is shown in Fig. 10. It can be observed from the Fig. that the density increases in the radial direction. This density variation is due to the centrifugal force that pushes the fluid away from the center.

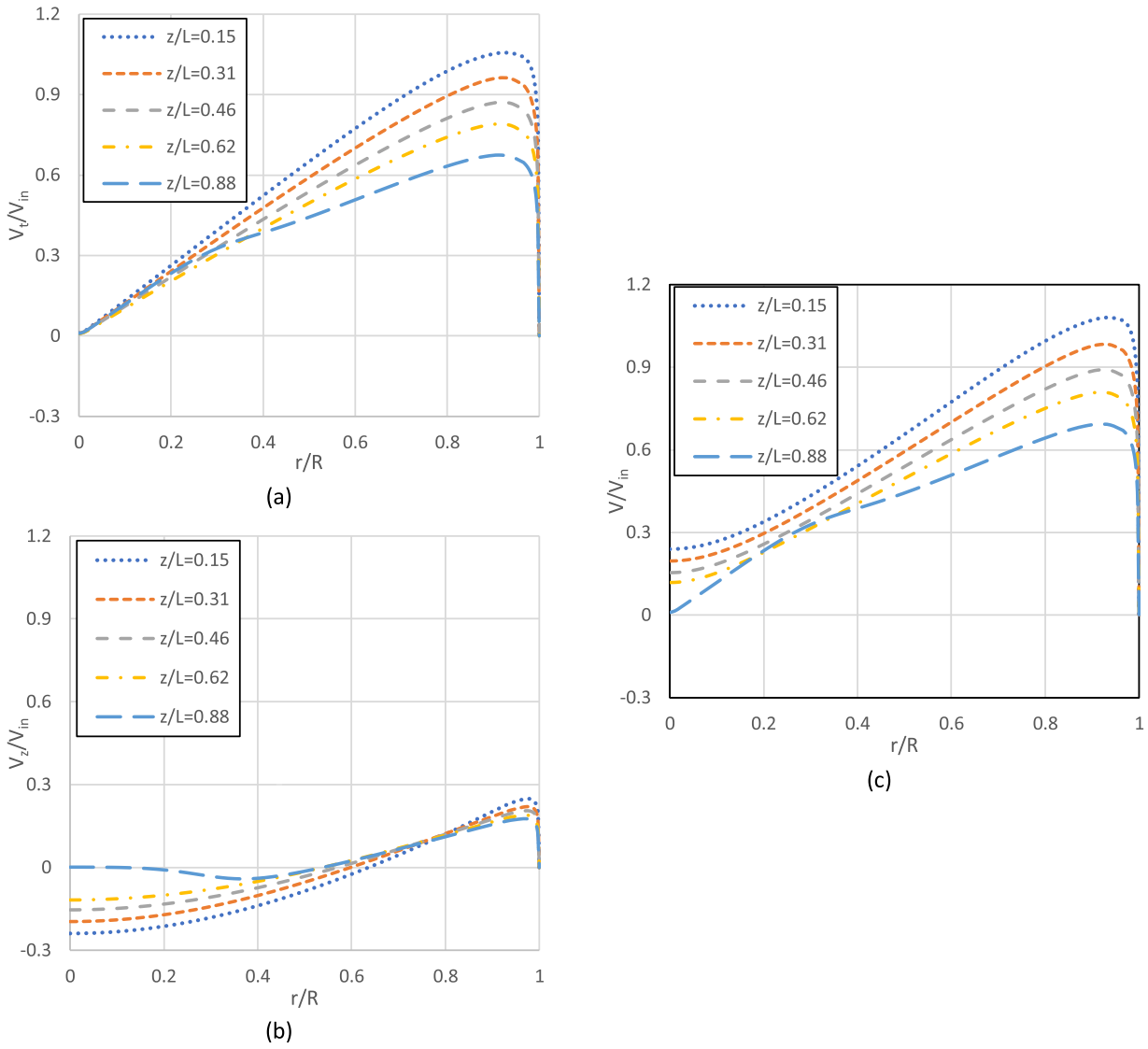

Fig. 7. Velocity profiles inside the vortex tube at different locations (a) tangential magnitude (b) axial velocity (c) total velocity.

From Fig. 9 (b), it can clearly be observed that the total pressure profile and the velocity have the same trend of increasing in radial direction to peak at the periphery. Then, the pressure decreases to reach to the static pressure at the wall surface due to no slip condition. It worth mentioning that, although the velocity magnitude decreases along the tube length, the total pressure increase in this direction. Hence, the static pressure change dominates that of the dynamic pressure as in Eq. 10.

$$P_{total} = P_{static} + \frac{\rho V^2}{2} \tag{10}$$

Fig. 11 (a) shows the radial variation of the static temperature at different locations in the VT. The temperature profile has a negative gradient in the radial direction, which indicates heat conduction

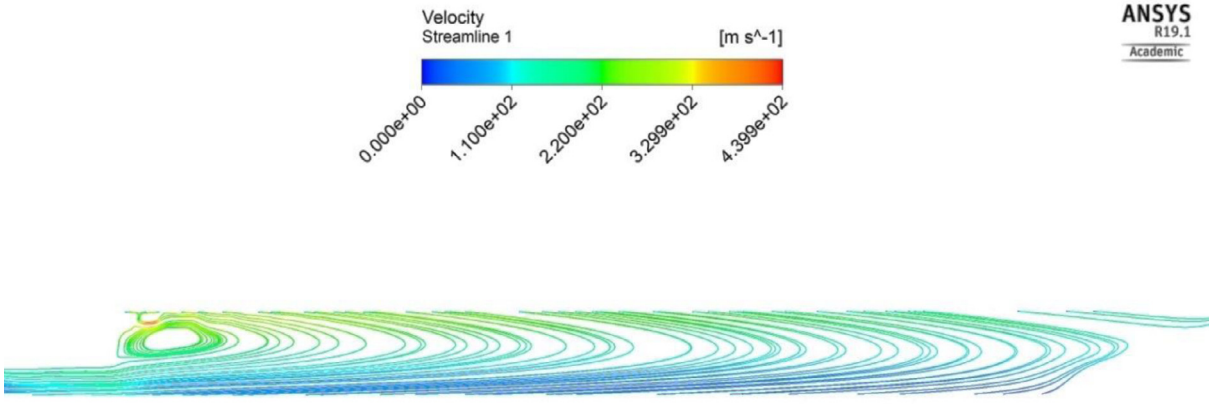

Fig. 8. Velocity streamlines at the periodic surface.

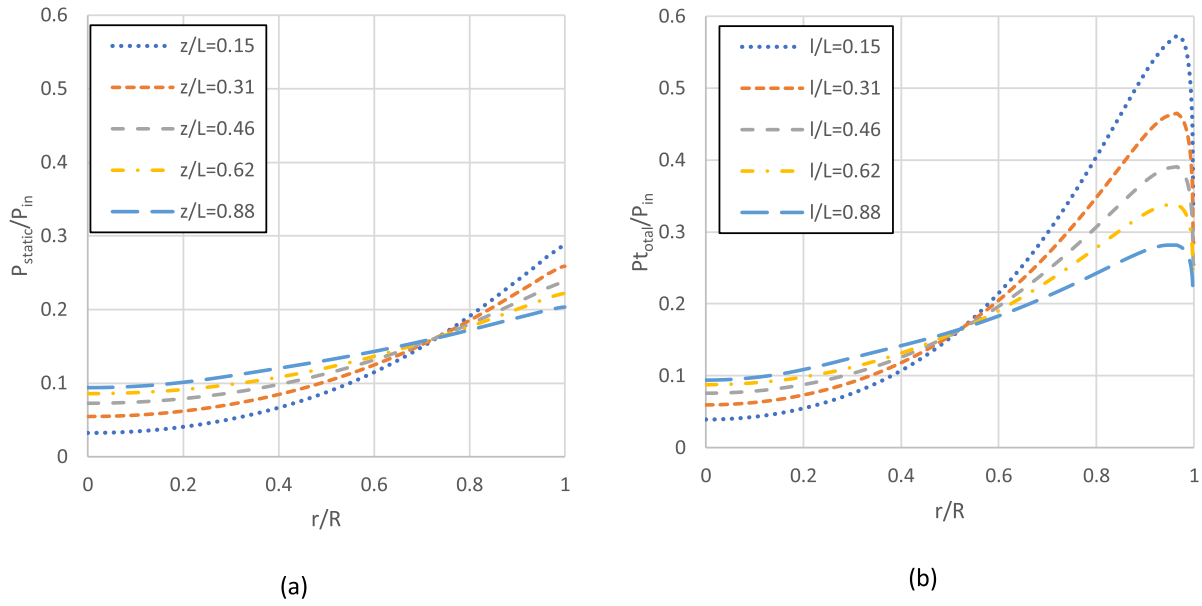

Fig. 9. Pressure profiles inside the vortex tube at different locations (a) static pressure (b) total pressure.

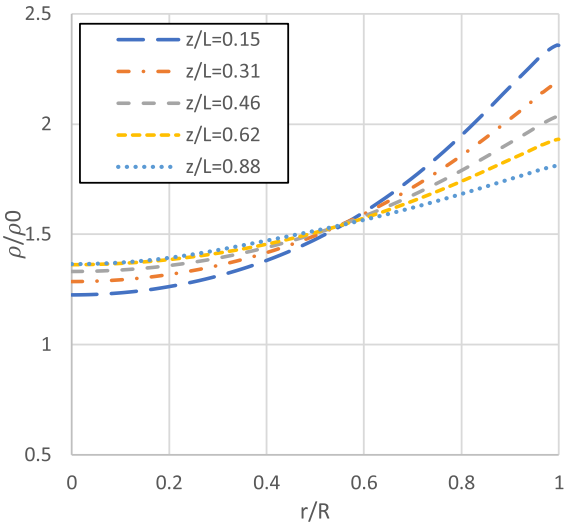

Fig. 10. Density profile inside the vortex tube at different locations.

from the near axis region to the peripheral region. This outcome is due to the contradicting effect of pressure and density on the static temperature as $T=P/(\rho R)$. The increase in the static pressure is not sufficient to accommodate the increase in density, which consequently leads to a decrease in the static temperature. As fluid flows towards the hot outlet, the amount of heat conducted radially decreases due to a lower temperature difference. For instance, at z/L=0.15, the radial temperature drop is about 10 K, while at z/L=0.88mm it is about 3 K. On the other hand, static temperature increases in the axial direction, which confirms that the heat is conducted from the hot to the cold outlet side. This heat transfer phenomena cannot be neglected, due to the nature of swirl flow in the VT. Swirl flow significantly increase the contact area and the residence time of fluid layers, hence the heat transfer between them. It worth noting that, the radial temperature drop violates the secondary flow theory. The theory claims that the secondary circulations work as a refrigeration cycle where it absorbs heat from the cold core (center) and reject it to the near wall region.

Fig. 11 (b) presents that the total temperature is the minimum at the center and increases in the radial direction. This profile is due to the nature of velocity distribution inside the VT. Despite of the velocity reduction, the total temperature increases in the axial direction. This contradiction is due to conversion of kinetic energy into heat by shear forces. At z/L=0.88mm, near the tip of the valve, the static and the total temperatures are equal because of the stagnation of the fluid at this region. Another remarkable outcome that should be pointed out is that at the near wall region with no slip condition, the static and total temperatures become equal as fluid flow along the tube, which is in agreement with the larger eddy simulation model in [34].

4. Conclusion

The flow field inside a real RHVT is investigated numerically using a three-dimensional standard $k-\varepsilon$ turbulence model. Velocity, pressure, and temperature radial profiles are plotted at various tube locations. These investigations enabled the following main conclusions to be drawn.

- Enhanced wall function gives more realistic results than the standard wall function, since it validates the fact that the total and static temperatures are equal at the wall surfaces of the tube at $Y^+ < 1$.
- The flow structure inside RHVT consists of a forced vortex that occupies a big portion of the fluid domain (from r/R=0 to 0.9) and a free vortex that exists at the periphery of the tube (from r/R=0.9 to 1).
- At the near wall region, the large velocity gradient of the tangential component enhance the transfer of the centrifugal force between fluid layers due to the shear stress and viscosity of the fluid.
- The axial velocity profile indicates that a large amount of fluid return towards the cold end, which decreases along the tube length. Also, a momentum transfer occurs from the near wall to the core region.
- The static and total pressures are equal at the wall surface due to no slip condition.
- In spite of the fact that pressure in the peripheral region is higher than that in the near axis region, the radial velocity component is very small due to the centrifugal force that pushes the fluid particles away from the center.
- The relation between the static pressure and temperature is not directly proportional. Therefore, in the high-pressure region a low

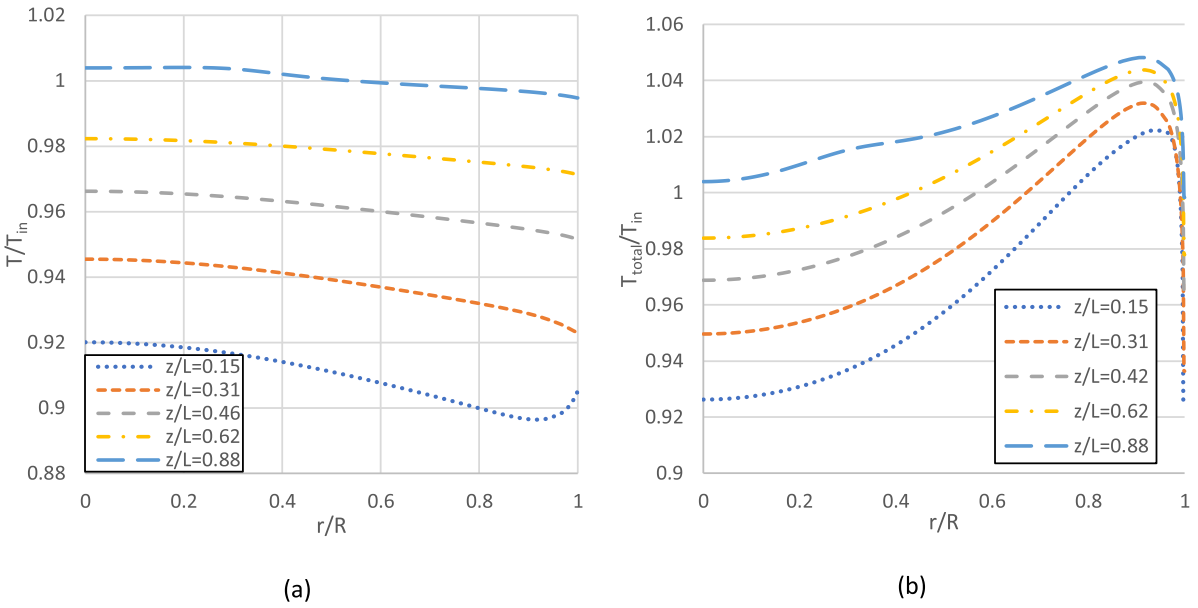

Fig. 11. Temperature profiles inside the vortex tube at different locations (a) static temperature (b) total temperature.

static temperature occur, while in the low-pressure region a high static temperature. This indirect relation emphasis the fact that the static pressure difference between center and the periphery of the tube cannot be considered as a cooling mechanism.

- Heat transfer occurs in two directions, radially from the center to wall and longtudinally from hot to cold outlet.
- Fluid expansion is the only cooling mechanism that is observed in the VT as the minimum temperature occurs only at the vortex generator region. Consequently, it is more convenient to regard a VT as a heater with heat separation capability.
- The relationship between cold mass fraction and outlet temperatures is non-monotonic. Therefore, an optimum value of the maximum hot and the minimum cold temperatures should be carefully evaluated as they were obtained at ε = 0.19 and 0.8 respectively.

Declaration of Competing Interest

The authors declare that they have no known competing financial interests or personal relationships that could have appeared to influence the work reported in this paper.

References

[1] R.D. Plant, M.Z. Saghir, Numerical and experimental investigation of high concentration aqueous alumina nanofluids in a two and three channel heat exchanger, Int. J. Thermofluids 9 (2021) 100055.
[2] M.O. Hamdan, S.-A. Al-Omari, A.S. Oweimer, Experimental study of vortex tube energy separation under different tube design, Exp. Therm. Fluid Sci. 91 (2018) 306–311.
[3] F. Alnaimat, I.M. AlHamad, B. Mathew, Heat transfer intensification in MEMS two-fluid parallel flow heat exchangers by embedding pin fins in microchannels, Int. J. Thermofluids 9 (2021) 100048.
[4] V. Guichet, N. Khordehgah, H. Jouhara, Experimental investigation and analytical prediction of a multi-channel flat heat pipe thermal performance, Int. J. Thermofluids 5 (2020) 100038.
[5] C. Pagkalos, et al., Evaluation of water and paraffin PCM as storage media for use in thermal energy storage applications: a numerical approach, Int. J. Thermofluids 1 (2020) 100006.
[6] G. Ranque, Experiments on expansion in a vortex with simultaneous exhaust of hot air and cold air, J. Phys. Radium 4 (7) (1933) 112–114.
[7] R. Hilsch, The use of the expansion of gases in a centrifugal field as cooling process, Rev. Sci. Instrum. 18 (2) (1947) 108–113.
[8] B. Alsayyed, M.O. Hamdan, S. Aldajah, Vortex tube impact on cooling milling machining, ASME International Mechanical Engineering Congress and Exposition, American Society of Mechanical Engineers, 2012.
[9] P.D. Kuila, S. Melkote, Effect of minimum quantity lubrication and vortex tube cooling on laser-assisted micromilling of a difficult-to-cut steel, Proc. Inst. Mech. Eng. (2020) 0954405420911268 Part B: Journal of Engineering Manufacture.
[10] X. Zhai, Research on the application of vortex tube type of cooling jacket in coal mine, AIP Conference Proceedings, AIP Publishing LLC, 2017.
[11] M. Izadi, et al., Optimizing the design and performance of solid–liquid separators, Int. J. Thermofluids 5 (2020) 100033.
[12] J. Chen, et al., Investigation of the convex mirror cooling of a transversely excited atmospheric (TEA) CO2 coaxial output unstable resonator laser, J. Opt. A Pure Appl. Opt. 11 (1) (2008) 015502.
[13] M.O. Hamdan, et al., Feasibility of vortex tube air-conditioning system, ASME/JSME Thermal Engineering Joint Conference, 2011.
[14] A.N. Shmroukh, M. Attalla, A.A.E.-N. Abd El, Experimental investigation of a novel sea water desalination system using ranque-hilsch vortex tube, Appl. Therm. Eng. 149 (2019) 658–664.
[15] Y. Xue, et al., Experimental investigation of the flow characteristics within a vortex tube with different configurations, Int. J. Heat Fluid Flow 75 (2019) 195–208.
[16] B.M. Dobratz, Vortex Tubes, a Bibliography, California. Univ., Livermore. Lawrence Radiation Lab, 1964.
[17] M. Kurosaka, Acoustic streaming in swirling flow and the Ranque—Hilsch (vortex-tube) effect, J. Fluid Mech. 124 (1982) 139–172.
[18] B. Parulekar, The short vortex tube, J. Refrigeration 4 (4) (1961) 74–80.
[19] P. Promvonge, S. Eiamsa-ard, Investigation on the vortex thermal separation in a vortex tube refrigerator, Science Asia 31 (3) (2005) 215–223.
[20] K. Dincer, S. Baskaya, B. Uysal, Experimental Investigation of the Effects of Length to Diameter Ratio and Nozzle Number on the Performance of Counter Flow Ranque–Hilsch Vortex Tubes, 44, Heat and Mass Transfer, 2008, pp. 367–373.
[21] S. Mohammadi, F. Farhadi, Experimental analysis of a Ranque–Hilsch vortex tube for optimizing nozzle numbers and diameter, Appl. Therm. Eng. 61 (2) (2013) 500–506.
[22] A. Celik, et al., The experimental investigation and thermodynamic analysis of vortex tubes, Heat Mass Transf. 53 (2) (2017) 395–405.
[23] M.O. Hamdan, et al., Experimental analysis on vortex tube energy separation performance, Heat Mass Transf. 47 (12) (2011) 1637–1642.
[24] V. Kırmacı, Exergy analysis and performance of a counter flow Ranque–Hilsch vortex tube having various nozzle numbers at different inlet pressures of oxygen and air, Int. J. Refrig. 32 (7) (2009) 1626–1633.
[25] H.R. Thakare, A.D. Parekh, Experimental investigation of Ranque—Hilsch vortex tube and techno–economical evaluation of its industrial utility, Appl. Therm. Eng. 169 (2020) 114934.
[26] H. Kaya, et al., Experimental analysis of cooling and heating performance of serial and parallel connected counter-flow Ranquee–Hilsch vortex tube systems using carbon dioxide as a working fluid, Int. J. Refrig. 106 (2019) 297–307.
[27] N. Aljuwayhel, G. Nellis, S. Klein, Parametric and internal study of the vortex tube using a CFD model, Int. J. Refrig. 28 (3) (2005) 442–450.
[28] H. Skye, G. Nellis, S. Klein, Comparison of CFD analysis to empirical data in a commercial vortex tube, Int. J. Refrig. 29 (1) (2006) 71–80.
[29] M. Baghdad, A. Ouadha, Y. Addad, Effects of kinetic energy and conductive solid walls on the flow and energy separation within a vortex tube, Int. J. Ambient Energy (2018) 1–17.
[30] R. Shamsoddini, A.H. Nezhad, Numerical analysis of the effects of nozzles number on the flow and power of cooling of a vortex tube, Int. J. Refrig. 33 (4) (2010) 774–782.
[31] M. Baghdad, et al., Numerical study of energy separation in a vortex tube with different RANS models, Int. J. Therm. Sci. 50 (12) (2011) 2377–2385.

[32] K. Dincer, et al., Experimental investigation of the performance of a Ranque–Hilsch vortex tube with regard to a plug located at the hot outlet, Int. J. Refrig. 32 (1) (2009) 87–94.
[33] A. Secchiaroli, et al., Numerical simulation of turbulent flow in a Ranque–Hilsch vortex tube, Int. J. Heat Mass Transfer 52 (23-24) (2009) 5496–5511.
[34] U. Behera, et al., CFD analysis and experimental investigations towards optimizing the parameters of Ranque–Hilsch vortex tube, Int. J. Heat Mass Transfer 48 (10) (2005) 1961–1973.
[35] T. Dutta, K. Sinhamahapatra, S. Bandyopdhyay, Comparison of different turbulence models in predicting the temperature separation in a Ranque–Hilsch vortex tube, Int. J. Refrig. 33 (4) (2010) 783–792.
[36] H.R. Thakare, A. Parekh, Computational analysis of energy separation in counter—flow vortex tube, Energy 85 (2015) 62–77.
[37] A. Bramo, N. Pourmahmoud, A numerical study on the effect of length to diameter ratio and stagnation point on the performance of counter flow vortex tube, Aust. J. Basic & Appl. Sci (10) (2010) 4.
[38] S. Eiamsa-ard, P. Promvonge, Numerical investigation of the thermal separation in a Ranque–Hilsch vortex tube, Int. J. Heat Mass Transfer 50 (5-6) (2007) 821–832.
[39] T. Farouk, B. Farouk, A. Gutsol, Simulation of gas species and temperature separation in the counter-flow Ranque–Hilsch vortex tube using the large eddy simulation technique, Int. J. Heat Mass Transfer 52 (13-14) (2009) 3320–3333.
[40] H. Khazaei, A.R. Teymourtash, M. Malek-Jafarian, Effects of gas properties and geometrical parameters on performance of a vortex tube, Scientia Iranica 19 (3) (2012) 454–462.
[41] M.O. Hamdan, B. Alsayyed, E. Elnajjar, Nozzle parameters affecting vortex tube energy separation performance, Heat Mass Transf. 49 (4) (2013) 533–541.
[42] U. Behera, et al., Numerical investigations on flow behaviour and energy separation in Ranque–Hilsch vortex tube, Int. J. Heat Mass Transfer 51 (25-26) (2008) 6077–6089.